Anal Bioanal Chem
DOI 10.1007/s00216-014-8158-0

RESEARCH PAPER

# A micropixelated ion-imaging detector for mass resolution enhancement of a QMS instrument

**Sarfaraz U. A. H. Syed · Gert B. Eijkel · Simon Maher · Piet Kistemaker · Stephen Taylor · Ron M. A. Heeren**

Received: 26 June 2014 / Revised: 29 August 2014 / Accepted: 2 September 2014
© Springer-Verlag Berlin Heidelberg 2014

**Abstract** An in-vacuum position-sensitive micropixelated detector (Timepix) is used to investigate the time-dependent spatial distribution of different charge state (and hence different mass-to-charge (*m/z*)) ions exiting an electrospray ionization (ESI)-based quadrupole mass spectrometer (QMS) instrument. Ion images obtained from the Timepix detector provide a detailed insight into the positions of stable and unstable ions of the mass peak as they exit the QMS. With the help of image processing algorithms and by selecting areas on the ion images where more stable ions impact the detector, an improvement in mass resolution by a factor of 5 was obtained for certain operating conditions. Moreover, our experimental approach of mass resolution enhancement was confirmed by in-house-developed novel QMS instrument simulation software. Utilizing the imaging-based mass resolution enhancement approach, the software predicts instrument mass resolution of ~1,0000 for a single-filter QMS instrument with a 210-mm long mass filter and a low operating frequency (880 kHz) of the radio frequency (RF) voltage.

Published in the topical collection *Mass Spectrometry Imaging* with guest editors Andreas Römpp and Uwe Karst.

**Electronic supplementary material** The online version of this article (doi:10.1007/s00216-014-8158-0) contains supplementary material, which is available to authorized users.

S. U. A. H. Syed · G. B. Eijkel · P. Kistemaker · R. M. A. Heeren (✉)
FOM Institute AMOLF, Science Park 104, 1098 XG Amsterdam, The Netherlands
e-mail: heeren@amolf.nl

S. Maher · S. Taylor
Department of Electrical Engineering and Electronics, University of Liverpool, Liverpool L69 3GJ, UK

**Keywords** Mass spectrometry · Imaging · Spectroscopy/instrumentation

## Introduction

Invented by Wolfgang Paul and Helmut Steinwedel in 1953 [1], a quadrupole mass spectrometer (QMS) instrument remains a widely used analytical tool for separating charged species in space according to their *m/z* ratio. The QMS contains three elements; (1) ion source, (2) quadrupole mass filter (QMF), and (3) ion detector [2]. The wide range of applications involving QMS in both industry and research give an impressive testimony to the value of this instrument. A simple QMF consists of four parallel electrodes, ideally of hyperbolic cross section, accurately positioned in a radial arrangement such that they are equally spaced about a central axis. However, for the ease of fabrication, circular electrodes are often used as they provide good approximation of the quadrupole field.

The resolution of a QMS directly relates to the rejection of unstable ions within the QMF. The behavior of the ions as they pass through the QMF can be described by the Mathieu equation. The stability (or boundedness) of solutions to Mathieu's equation, as a function of dimensionless parameters ($a$, $q$), are characterized by transition curves. When plotted in $a$-$q$ space, the areas under overlapping transition curves represent regions of stability in two dimensions ($x$ and $y$). This plot is commonly referred to as the Mathieu stability diagram [2–4]. The lower stability region of the Mathieu diagram (Closest to the origin) is normally used in mass filter operation showing iso-β lines for the $x$ and $y$ directions and a typical scan line are shown in Fig. S1 in the Electronic supplementary material (ESM). The ratio of the direct current (DC) voltage $U$ and radiofrequency (RF) voltage $V$ controls the QMF resolution setting and the voltage $V$ sets the mass scale. Varying $V$

Published online: 01 October 2014

and $U$ (while keeping the ratio of $U$ to $V$ constant) changes the mass value that can successfully pass through the filter. This variation of the voltages is called the mass scan line. When $a \neq 0$, only those ions with operating points lying between the intersections of the mass scan line with $\beta_y=0$ and $\beta_x=1$ will have stable trajectories in both $x$ and $y$ directions. With increase in the $U/V$ ratio, the mass scan line approaches to the tip of the stable region and only a narrow range of $m/z$ values will have stable trajectories, hence resolution increases. Nevertheless, it should be noted that the stability diagram is an ideal case and is true for an infinite-length QMF. In practice, because of finite length, the resolution of the QMS is limited by the number ($N$) of RF cycles an ion experiences in the quadrupole field. $N$ may be calculated by: $N=(f\,l)/\sqrt{(2E_z/m)}$ where $l$ is the length of the mass filter, $f$ is frequency of the RF voltage, and $E_z$ the ion energy. From the mass spectrum obtained, the resolution $R$ can be calculated by using the equation $R=M/\Delta M$, where $M$ is the mass-to-charge value of the given spectral peak and $\Delta M$ is the width of the mass peak measured using either 10 or 50 % peak height definition.

In the past, many workers investigated the factors that influence resolution of a QMS and conditions that can be applied to improve it. Brubaker and Tull investigated the dependence of transmission efficiency and resolution of a QMS on ion-source exit aperture and frequency of excitation [5]. It was concluded that higher resolution is obtained with small aperture size and higher frequency. In 1971, Holme et al. performed a series of experiments to investigate the factors which determine the resolution of a QMF under normal operating conditions and derived the empirical relationship $R=N^n/K$; where $n$ is either or exactly equal to 2 and $K$ is a constant which is assumed to be 20 for all practical purposes [6]. However, recently it has been shown that the resolution will saturate with increasing the number of RF cycles and thus the theoretical maximum resolution is limited by the intersection of the mass scan line with the stability zone [7]. The relationship $R=N^n/K$ is only valid for an ideal case. There have been several investigations of QMS operation in higher stability regions with higher $a$ and $q$ values [8, 9]. In general, operation in higher stability zones increases resolution but requires larger voltages. Recently, application of static magnetic field ($\boldsymbol{B}$) to the body of QMF was found to enhance the instrument resolution and transmission under different operating conditions and is described in [10, 11].

In our previous work [12], we have presented a novel instrument assembly consisting of an electrospray ionization (ESI)-based QMS coupled with a Timepix detector for investigation of the two-dimensional (2D) beam profile exiting the QMS in RF only mode and selective ion transmission mode of operation. In this paper, we have investigated in detail the time-dependent spatial distribution of ions exiting the QMS in selective ion transmission mode (mass filtering), and the knowledge obtained from this investigation is applied to improve mass resolution.

## Methods

### Experimental method

Measurements were taken using the instrument described in [12]. The description of the system is reproduced here for completeness. Figure S2 in the ESM shows a 2D schematic diagram with visualization of different potentials used in the system. The microchannel plate (MCP)/Timepix detector, mounted on a vacuum flange, is placed inside the vacuum chamber 8 cm from the exit side of the QMF (Quadrupole ABB Extrel, from Extrel, Pittsburgh, USA). Ions are created by ESI. In all the experiments reported in this paper, the analyte was a 10-μM solution of bovine cytochrome $c$ (Sigma Aldrich) in 50/50 water/methanol (by volume) with 0.1 % formic acid to aid protonation.

The octopole is used to interface the ESI ion source and the quadrupole mass spectrometer. The octopole has an electrode radius of 3 mm, length 170.5 mm, and an inscribed field radius of 4.5 mm. The RF potential on the octopole was maintained at 50 $V_{0\text{–peak}}$, and the RF frequency was set at 1 MHz. The kinetic energy of ions entering the QMS will be influenced mainly by four factors: the capillary potential (120 V), the skimmer potential (25 V), the energy loss by collisions with background gas, and the DC bias applied to the octopole. Ions with sufficient energy travel into the quadrupole mass filter, which can either operate in transmission only mode (RF only mode) or mass selective ion transmission mode. There is an ion lens assembly between the octopole and QMF, an exit electrode to the octopole, and an entrance electrode to QMF, which were all maintained at ground potential. The aperture diameter of both lens electrodes is 2 mm. Between QMF and MCPs, there is an exit electrode to the QMF followed by an Einzel lens assembly, which were all maintained at ground potential. The aperture diameter of the exit electrode to the QMF is ≈8.5 mm. The QMF has a mass range of up to 4,000 $m/z$, a length of 210 mm, an electrode diameter of 9.525 mm, an inscribed field radius of 4.17 mm, and an operating frequency of 880 kHz. The pressure at the octopole section was $5.0\times10^{-4}$ mbar, and the operating pressure of the QMF section was $6.4\times10^{-6}$ mbar.

A chevron MCP stack (active area $\phi$=4 cm, 12 μm pores, 15 μm pitch; F2225-21N290, Hamamatsu Photonics Deutschland GmbH, Herrschingam Ammersee, Germany) is placed in front of the Timepix chip array. Ions exiting from the quadrupole will impact on the MCPs, and the resultant electron shower is projected on the Timepix chips. The dimension of an individual Timepix chip is $1.4\times1.6$ cm$^2$. The major characteristics of this application-specific integrated circuit (ASIC) are 256×256 pixels of 55×55 μm each per chip, low electronic

noise, and pixel level functionality. In the work reported, we have employed an array of 2×2 Timepix chips. The front MCP was maintained at −1850 V, the back MCP at −400 V, and the Timepix detector was at ground potential. Timepix data is then acquired by the dedicated Pixelman software package. With this setting for each ion impact, $6\times10^5$ electrons are generated which are projected on about four detector pixels. A detector pixel requires about 600 electron charges to register one count. That means that for one impacting ion, 4 pixels are activated and the spatial resolution is less than 0.1 mm.

Data and image analysis were performed using software developed in MATLAB-R2011b (Mathworks, Natick, USA). The QMS assembly was controlled with the in-house-developed AWG software with a fully automated data acquisition electronic drive unit for scanning of the mass filter electrode voltages. To obtain a mass spectrum, the QMS scan steps and the Timepix integration/read-out times are synchronized. The data of every measurement frame is saved in a separate sparse data file that contains the pixel address and the corresponding ion hits recorded by each pixel. Mass spectra are built by using the summed signals per frame. The spectrum is mass calibrated using the set mass range of the QMS. It should also be noted that the QMS has a mass resolution of approximately 2.3 Da full-width half maximum (FWHM). The *U/V* ratio was set at ≈0.168. The mass resolution is limited due to finite number of RF cycles the ion experiences in the quadrupole field.

## Software

### *Resolution per pixel approach*

A MATLAB script was developed to determine the areas with highest mass resolution within the ion beam projection. The FWHM resolution $M/\Delta M$ was calculated for a chosen mass for each pixel (i.e., spectrum) and displayed as a 2D resolution surface image. Consequently, the region that showed the highest resolution was selected and the spectra from the selected pixels were summed. The resulting spectrum was compared with the spectrum obtained by summing the full beam projection area. The full height was defined as the intensity difference between the lowest and highest intensity in the

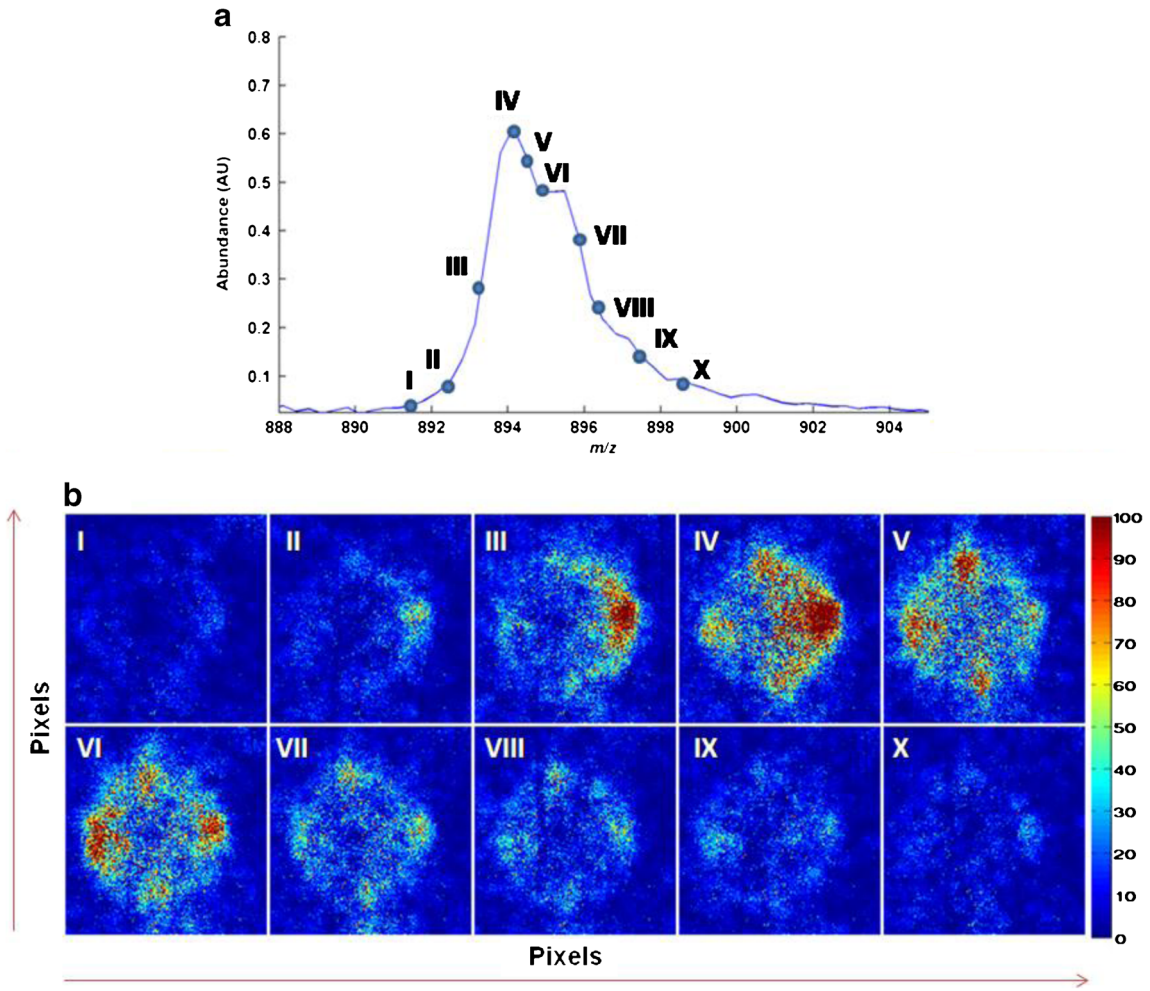


**Fig. 1** **a** Mass peak of $[M+14H]^{14+}$ charge state of cytochrome *c*. **b** Normalized 2D contour maps of different points of the mass speak highlighted in (**a**)

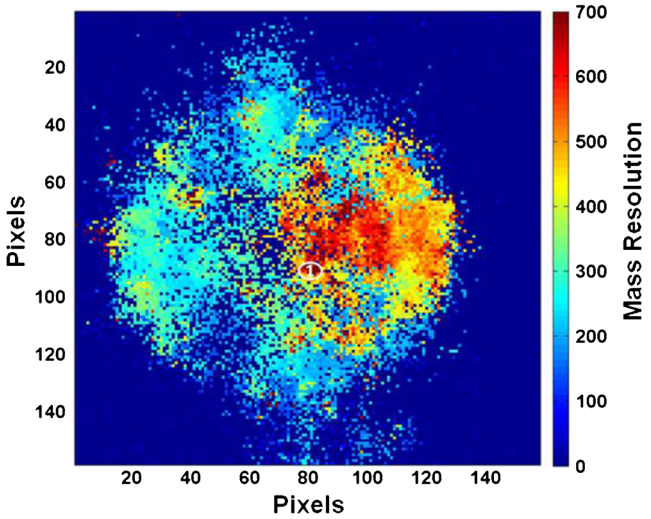


**Fig. 2** Variation of mass resolution (FWHM) measured per pixel at across ion beam of $[M+14H]^{14+}$ charge state of cytochrome c

spectral window around the peak of interest for the calculation of the FWHM. $M$ is the $m/z$ channel at the peak summit, $\Delta M$ the peak width at 50 % full height, interpolated between adjacent measurement points.

*Concentric rings approach*

A data set of 100 spectra was constructed to compare the spectral features with respect to the distance from the axis of the ion beam. The spectra were created by averaging the pixels that are positioned on concentric rings around the central axes of the ion beam projection. From the center position (pixel 1, spectrum 1), the spectra positioned on concentric rings with a radius increasing from 1 to 100 pixels were summed and averaged. A graphical description of this approach is provided as S3 in the ESM.

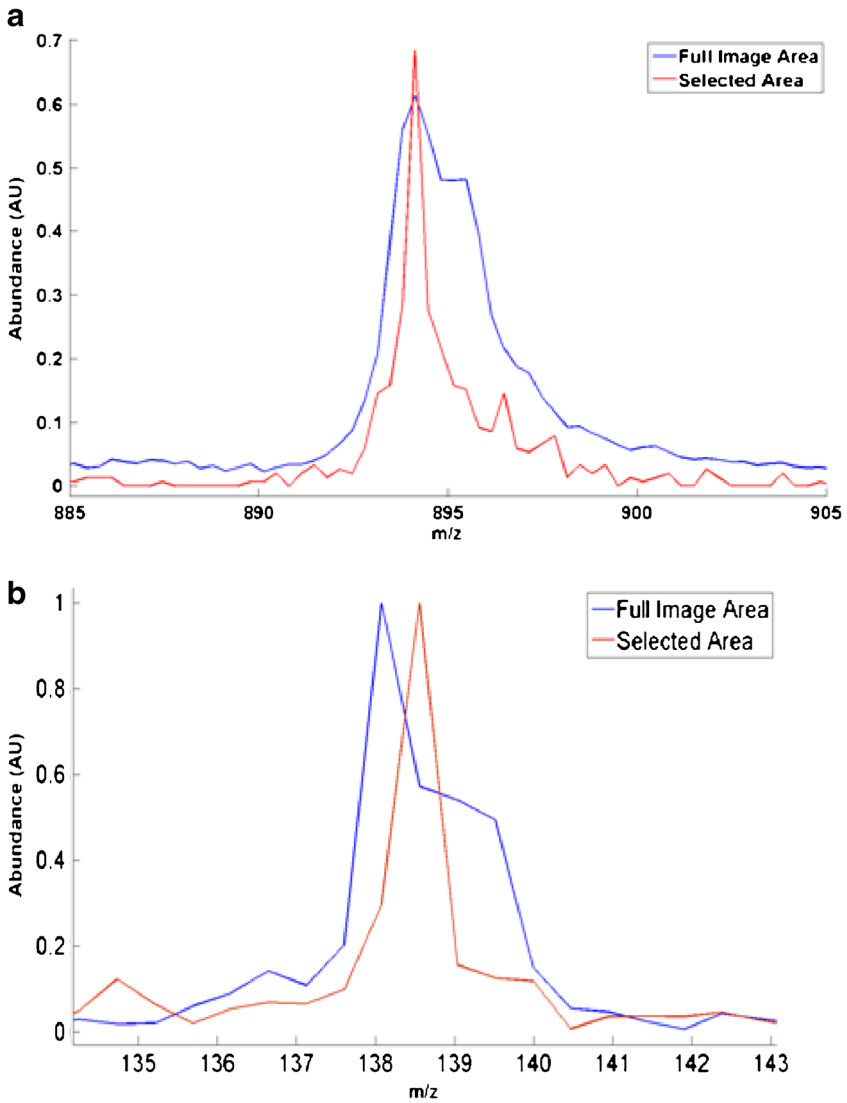


**Fig. 3** **a** Comparison of mass spectrum of entire image area of $[M+14H]^{14+}$ charge state of cytochrome c with highlighted area (1) of Fig. 2; **b** Comparison of mass spectrum of entire image area of a Caffeine fragment ion with selected enhanced mass resolution area

*QMS2 imaging*

A custom software program (QMS2 Imaging) developed in Visual C++ environment was used for simulating QMS instrument. The program calculates ion trajectories by solving the Mathieu equations using a fourth-order Runge–Kutta algorithm. Our numerical approach has been described previously [10, 11]. It operates by dividing the ion trajectories into small time steps and assuming that over the steps the ion motion in three directions $x$, $y$, and $z$ is uncoupled. Mass scans are computed by ramping the values of $U$ and $V$ with fixed $U/V$ ratio, which sets the resolution of an instrument. The original model has been modified and upgraded to plot spatial distribution of individual ions exiting the mass filter by means of tracing the exit position in the $x$-$y$ plane. The final $x$, $y$ (and also $m/z$) information of each ion which successfully traverses the QMF is stored. The position information ($x$, $y$) is for the ion at the end of the length of the electrodes

A second program (IonSrc) allows entry conditions for a large number of ions (typically $10^8$), to be specified, which are subsequently supplied to the mass filter calculation engine to simulate individual trajectories in each case. Finally, MATLAB was used to postprocess the data and for the generation of graphical results.

## Results and discussions

Experimental results

*Time-dependent spatial distribution of ions exiting the QMS*

Figure 1a shows Timepix-generated mass peak of cytochrome $c$ charge state $[M+14H]^{14+}$. In Fig. 1a, even though the QMS was operated at a high-resolution setting (near the tip of the stability diagram), the mass resolution was limited because of the following reasons:

1. Ions experienced a finite number of RF cycles ($N$=77).
2. Mass peak is a convolution of many isotopes of charge state $[M+14H]^{14+}$ of cytochrome $c$, resulting in a broader mass spectrum.
3. Commercial QMS systems use circular electrodes, and though it provides good approximation to the quadrupole field, it is not an ideal hyperbolic field. This can result in a curved apex of the stability diagram rather than a sharp one. This increases the chance of acceptance of unstable ions and lowers resolving power.

Figure 1b shows a sequence of "contour" maps that indicate where the ions are transmitted by the QMS as it scans along the mass peak shown in Fig. 1a. We have described in our previous

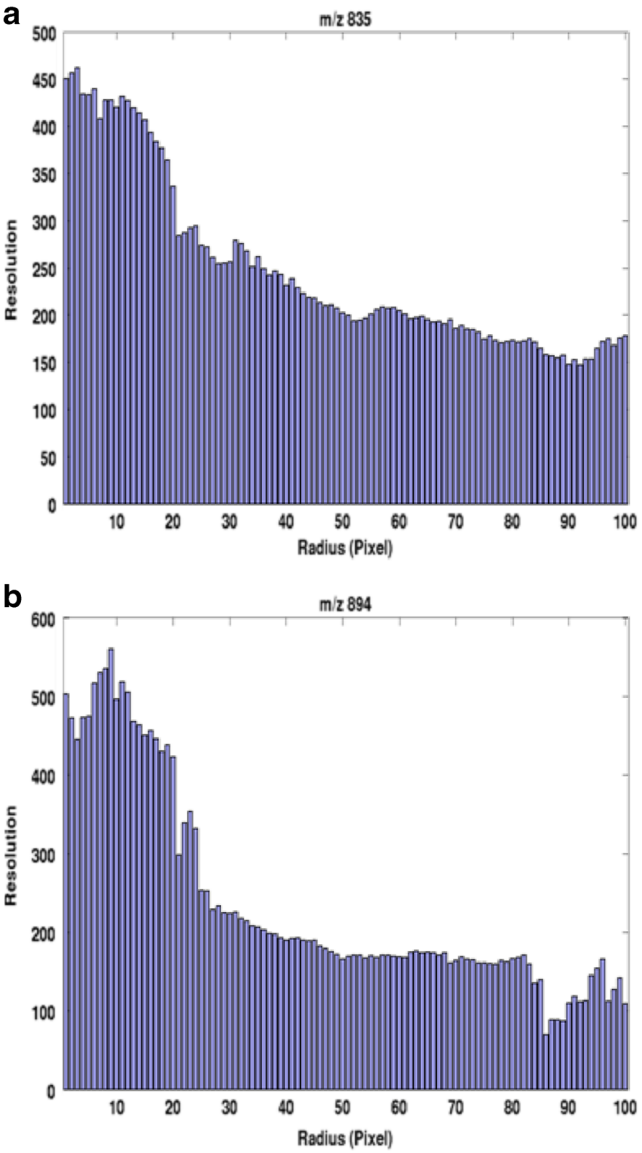


**Fig. 4** **a** Variation of mass resolution with increasing pixel radius for $m/z$ 835. **b** Variation of mass resolution with increasing pixel radius for $m/z$ 894

work [12] the 2D spatial distribution of different charge states (hence different $m/z$) of cytochrome $c$ complex mass spectrum, and it should be noted that the attention is given to the intense part of the beam. As seen from Fig. 1b, ions at the peak onset (i.e., I and II) of the mass spectrum are scattered everywhere. A large proportion of ions at the middle of the low mass tail and peak of the mass spectrum (III and IV) lie close to the positive $x$-axis with respect to the center of the beam. As the QMS scan moves further, ions from the beginning of the high mass tail to the peak offset ($V$ to $X$) lie in a region closer to ($x$, $y$) axis. Furthermore, it has to be realized that the observed ion distribution depends critically on the proper setting of the QMS. Small deviations from the optimal RF and DC setting can lead to differences in ion intensity distribution in the $x$-coordinate axis relative to the $y$-coordinate axis. Hence, the pattern differs for different voltage settings.

*Mass resolution enhancement using time-dependent spatial distribution*

With the help of information from Fig. 1 (i.e., where stable ions (ions at the peak) and unstable ions (ions on either side of the peak) impact the detector) and by using the described resolution per pixel algorithm in the software section, the obtained ion beam is scanned for mass resolution (FWHM) values at different areas on the ion image. Figure 2 shows a mass resolution plot on the ion image, and as seen from the figure, mass resolution is higher in regions closer to the *x*-axis, where the majority of the ions closer to the peak of the spectra lie. Figure 3a shows a comparison of mass spectra for the full ion beam image with the area highlighted as 1 in Fig. 2.

As seen from Fig. 3a, for the area highlighted as 1 in Fig. 2, there is a reduction in the low mass tail and high mass tail of the mass spectra, thus giving an improvement in mass resolution from ($R$=331 to $R$=1900). The reduction in mass tailing arises because of the reason that on the selected area of the detector, the majority of the impacted ions are from the peak of the mass spectrum (Fig. 1). It should also be noted that the mass spectra in Fig. 3 are normalized. To confirm this enhancement for lower *m/z*, we obtained a mass spectrum for a caffeine fragment ion, and Fig. 3b shows the comparison of selected area mass peak to full-image mass peak. The approach works fine with lower *m/z* too; the highest intense isotope peak at *m/z* 138.1 was shown to illustrate the mass resolution enhancement effect.

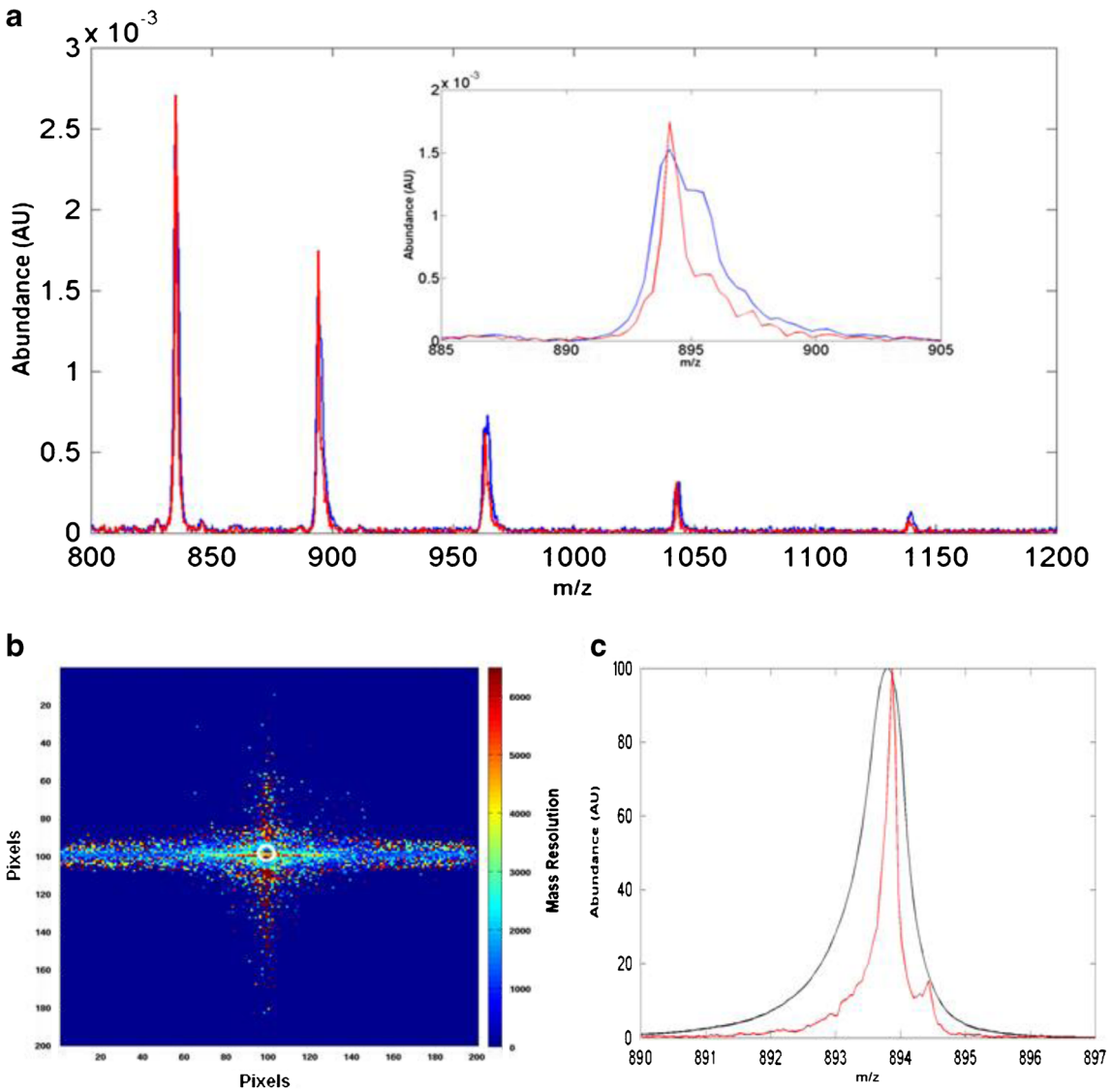


**Fig. 5** **a** Comparison of the measured mass spectrum of entire image area (*blue line*) with concentric ring area (*red line*) at pixel radius 9, shown in inset is zoomed in peak of $[M+14H]^{14+}$ charge state of cytochrome c. **b** Variation of mass resolution (FWHM) measured per pixel at across ion beam of the simulated *m/z* 894 peak with concentric ring of pixel thickness 1 highlighted (*white*). **c** Comparison of the simulated mass spectrum of entire image area (*black line*) with concentric ring area (*red line*) for *m/z* 894

*Mass resolution enhancement by using concentric radial rings approach*

Concentric rings of 1 pixel thickness on Timepix chip with increasing radius are picked to calculate the radial mass resolution distribution, and the mass spectra of ions impacting the area lying within the concentric ring are generated and mass resolution is calculated at FWHM. Figure 4a shows variation of mass resolution at FWHM with increasing pixel radius for *m/z* 835; whereas, Fig. 4b shows variation for *m/z* 894. As seen from Fig. 4, the resolution decreases as the concentric ring area is moved further away from the center of the image. The resolution is more pronounced at concentric ring areas with radius less than 20 pixels from the center. Figure 5a shows a comparison of mass spectra for the full ion beam image with the mass spectrum obtained for the selected concentric ring of pixel radius 9 and pixel thickness 1 on the image (shown in the inset is the zoomed in *m/z* 894 mass peak). As seen from the inset of Fig. 5a, there is a reduction of the low mass tail as well as high mass tail of the *m/z* 894 mass peak and the mass resolution measured at FWHM was found to be enhanced by more than a factor of 2.

The increase is resolution can be attributed to two factors:

1. With respect to the center of the quadrupole axis, the amplitude of ion trajectories in *y* direction of unstable ions is much higher compared with that of stable ions. So, more stable ions impact the regions closer to the center of the ion beam.
2. The radial distribution observed in [12] may also be contributing to this mass resolution enhancement effect, but it cannot be quantified.

Simulation results

To confirm our experimental observations, we simulated *m/z* 894 for a 1,000 mass resolution QMF at FWHM for ideal operating conditions (hyperbolic cross-section

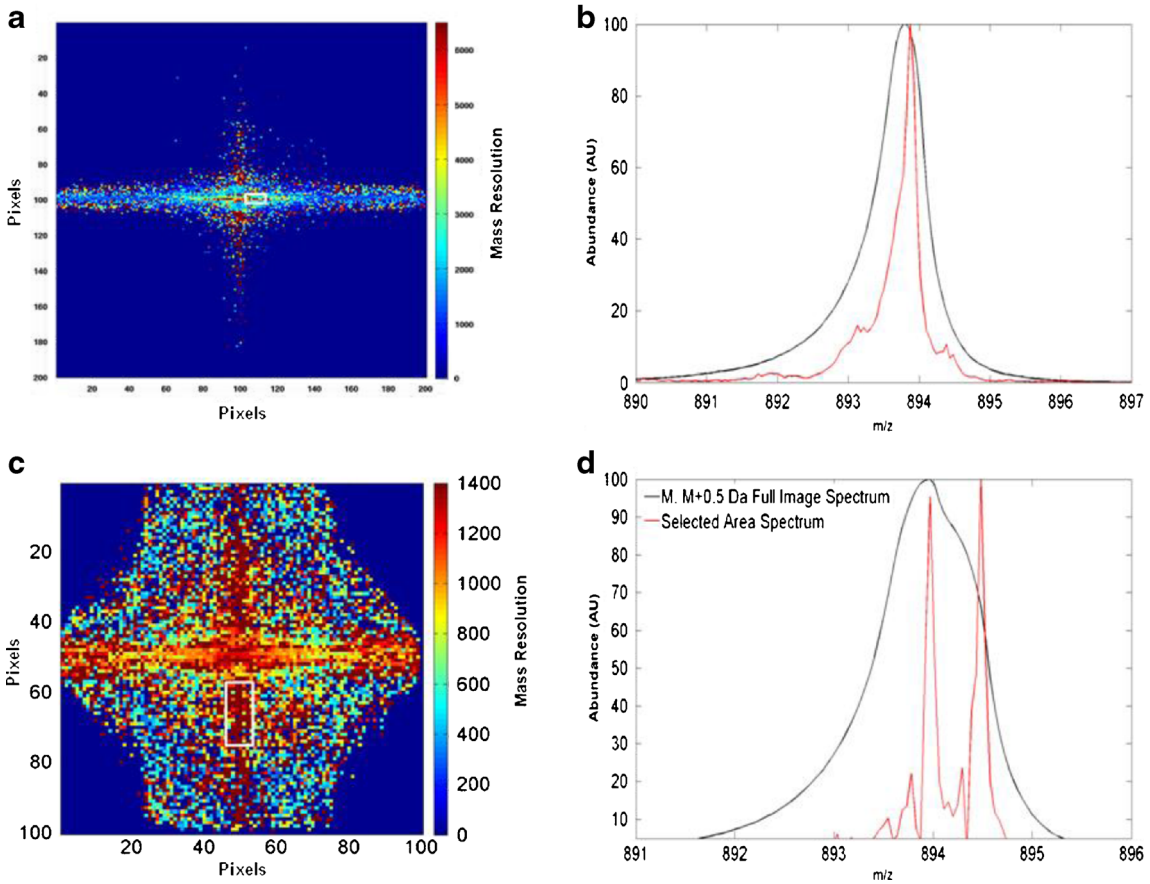


**Fig. 6** **a** Variation of mass resolution measured per pixel across ion beam of the simulated *m/z* 894 peak with a rectangular area highlighted (*white line*). **b** Comparison of the simulated mass spectrum of entire image area (*black line*) with mass spectrum of ions lying within the highlighted rectangular area in (**a**). **c** Variation of mass resolution measured per pixel across ion beam of the simulated *m/z* 894 and 894.5 mass peaks with a rectangular area highlighted (*white line*). **d** Comparison of the simulated mass spectrum of entire image area (*black line*) with mass spectrum of ions lying within the highlighted rectangular area in (**c**)

electrodes). All the simulations use 150 steps across the mass range with $5\times10^5$ ions injected and traced at each mass step. Mass peaks for *m/z* 894 are generated for a hyperbolic QMF with inscribed radius (field radius) of 4.17 mm and length 210 mm. The QMF was simulated at $N=82$ to give a mass resolution higher than 1,000 at FWHM. The MATLAB script uses zonal statistics to determine regions where the ions are located. Essentially this is an "imaginary" 2D grid. Information is then collated regarding the ions in each grid location. Note: the grid size (and hence number of grid "boxes") can be altered, grid is a representation of a pixel on the Timepix detector.

Figure 5b shows a resolution per pixel plot of the simulated data with a white color concentric ring highlighted. Figure 5c shows comparison of mass spectra for the full ion beam image with the mass spectrum obtained for the ions lying on the selected concentric area of pixel thickness 1 on the simulated exit position grid as shown in Fig. 5b. It should also be noted that each simulated mass spectrum is normalized with respect to peak intensity of the full-image-simulated mass spectrum. As seen from Fig. 5c, there is a reduction in low mass tail as well as high mass tail of the mass peak and the mass resolution is improved by a factor of 3.5 ($R_{\text{fullimage}}$=1,117 to $R_{\text{selected}}$= 3,909).

Figure 6a shows a resolution per pixel plot of the simulated data with a rectangular area highlighted. Figure 6b shows a comparison of mass spectrum for the full ion beam image with the mass spectrum obtained for the ions lying within the selected area on the ion beam image (as highlighted in Fig. 6a). There is an improvement in mass resolution of the selected area mass peak by a factor of 2.9 ($R_{\text{fullimage}}$=1,117 to $R_{\text{selected}}$=3,239) upon comparison with a mass spectrum of the full ion beam image.

For a better illustration of this mass resolution enhancement approach, *m/z* 894 was simulated along with *m/z* 894.5 Da (M+0.5). The mass resolution was insufficient to separate the two mass peaks. The simulated mass spectrum of the convoluted peaks is shown in Fig. 6d (black line). Using the resolution per pixel approach, a rectangular area that has high mass resolution compared with full the image was selected (Fig. 6c), and the comparison of full-image mass spectrum (black line) and selected area mass spectrum (red line) is shown in Fig. 6d. It can be observed that the minimum mass resolution required to separate M and M+0.5 Da peaks is achieved. The mass resolution of selected area for individual mass peak is greater by a factor of 8.5 ($R_{\text{fullimage}}$=1,117 to $R_{\text{selected}}$=9,494).

## Conclusions

Via Timepix detector, we have shown experimentally for the very first time how the time-dependent spatial distribution of the ion beam exiting the QMS varies as it is scanned, thus giving information about the impact positions of stable and unstable ions. We presented two novel image processing approaches that can be applied to experimental data to obtain enhancement of mass resolution based on the measured spatial distribution. An enhancement in mass resolution by a factor of 5 was obtained experimentally for certain operating conditions.

Our experimental observations were confirmed by in-house-developed novel QMS2-imaging software. The software predicts instrument mass resolution of 10,000 at FWHM via a single-filter QMS, and by application of the mass resolution enhancement approach, which if realized in practice will enable a greater range of applications for quadrupole based instruments.

**Acknowledgments** This work is part of the research program of the Foundation for Fundamental Research on Matter (FOM), which is part of the Netherlands Organisation for Scientific Research (NWO). The research is supported by the Comprehensive Analytical Science and Technology (COAST) foundation, which is the assigned program committee in the NWO Technology Area for Sustainable Chemistry (TASC) program. The authors acknowledge Ronald Buijs and Marc Duursma, of AMOLF for their contribution to the experiments.

## References

1. Paul W, Raether M (1955) Das elektrische massenfilter. Z Phys 40: 262–273
2. Dawson PH (1976) Quadrupole mass spectrometry and its applications. Elsevier, Amsterdam
3. March RE, Todd JFJ (2005) Quadrupole ion trap mass spectrometry. Wiley, New Jersey, pp 43–47
4. Batey JH (1987) Quadropole gas analysers. Vacuum 37:659–668
5. Brubaker WM, Tuul J (1964) Performance studies of a quadrupole mass filter. Rev Sci Instrum 35(8):1007–1010
6. Holme AE, Thatcher WJ, Leck JH (1972) An investigation of the factors determining maximum resolution in a quadrupole mass spectrometer. J Phys E Sci Instrum 5:429–433
7. Syed S, Hogan T, Gibson J, Taylor S (2012) Factors influencing the QMF resolution for operation in stability zones 1 and 3. J Am Soc Mass Spectrom 23:988–995
8. Hiroki S, Abe T, Murakami Y (1994) Detection of a 10–4 helium peak in a deuterium atmosphere using a modified high-resolution quadrupole mass spectrometer. Rev Sci Instrum 65(6):1912–1917
9. Du Z, Douglas DJ, Konenkov N (1999) Elemental analysis with quadrupole mass filters operated in higher stability regions. J Anal At Spectrom 14(8):1111–1119
10. Maher S, Syed S, Hughes DM, Gibson JR, Taylor S (2013) Mapping the stability diagram of a quadrupole mass spectrometer with a static transverse magnetic field applied. J Am Soc Mass Spectrom 24(8): 1307–1314
11. Syed S, Maher S, Taylor S (2013) Quadrupole mass filter operation under the influence of magnetic field. J Mass Spectrom 48(12):1325–1339
12. Syed S, Eijkel G, Kistemaker P, Ellis S, Maher S, Smith D, Heeren R (2014) Experimental investigation of the 2D ion beam profile generated by an ESI Octopole-QMS system. J Am Soc Mass Spectrom 25(10):1780–1787. doi:10.1007/s13361-014-0958-0

**Analytical and Bioanalytical Chemistry**

**Electronic Supplementary Material**

# A micropixelated ion-imaging detector for mass resolution enhancement of a QMS instrument

Sarfaraz U. A. H. Syed, Gert B. Eijkel, Simon Maher, Piet Kistemaker, Stephen Taylor, Ron M. A. Heeren

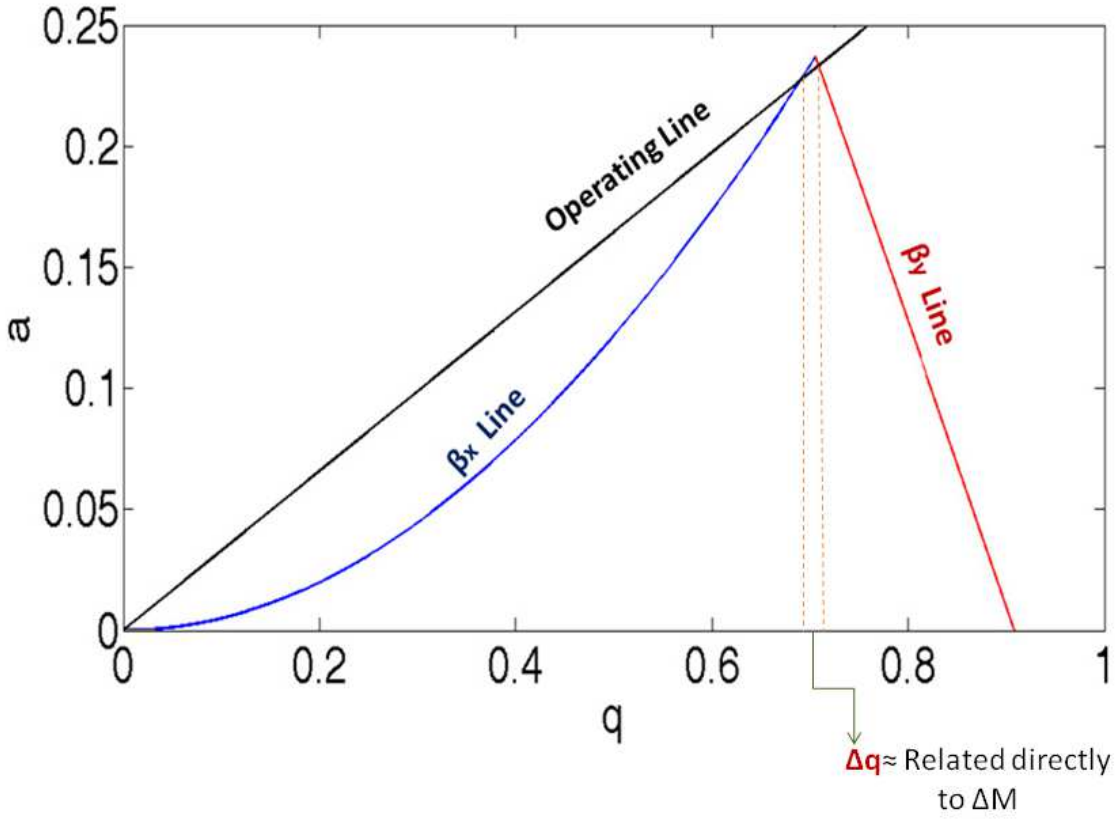


**Fig. S1** The Mathieu stability diagram for zone 1 with the intersection of the scan line at *U/V* < 100%

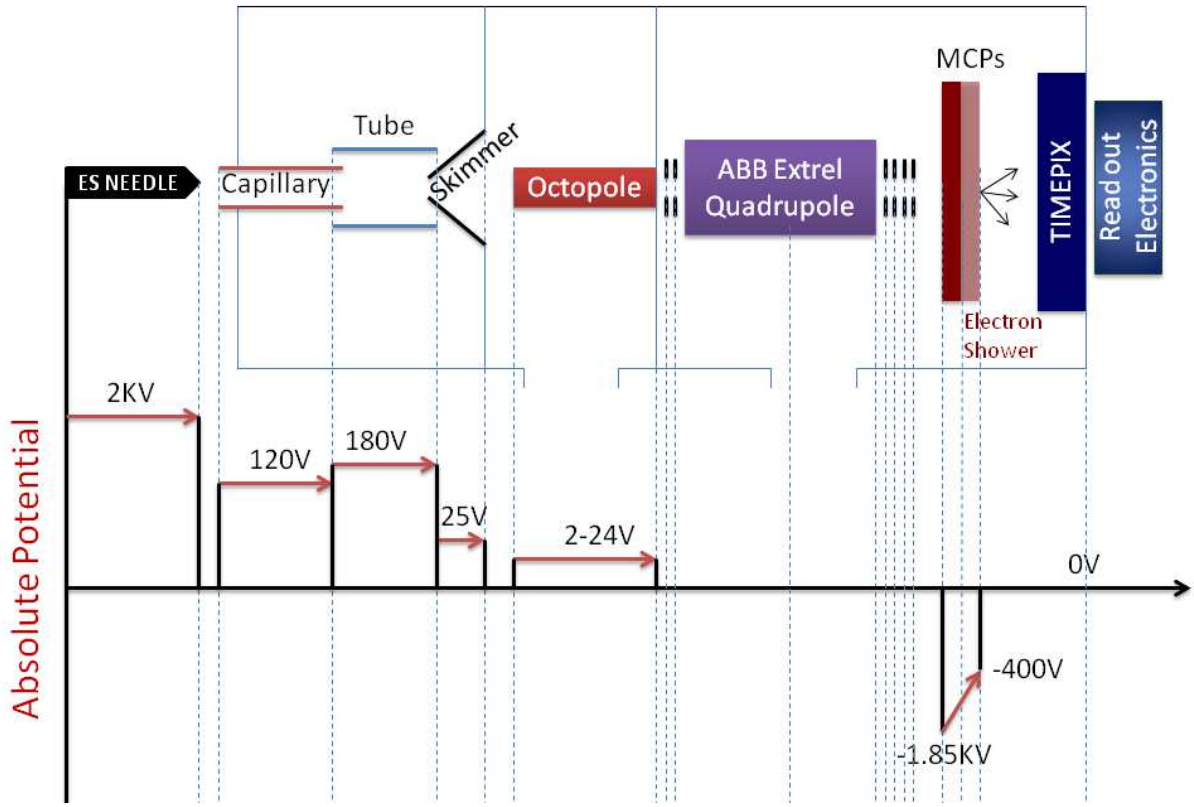


**Fig. S2** 2D schematic diagram of the experimental setup with visualization of absolute potential distribution of the system

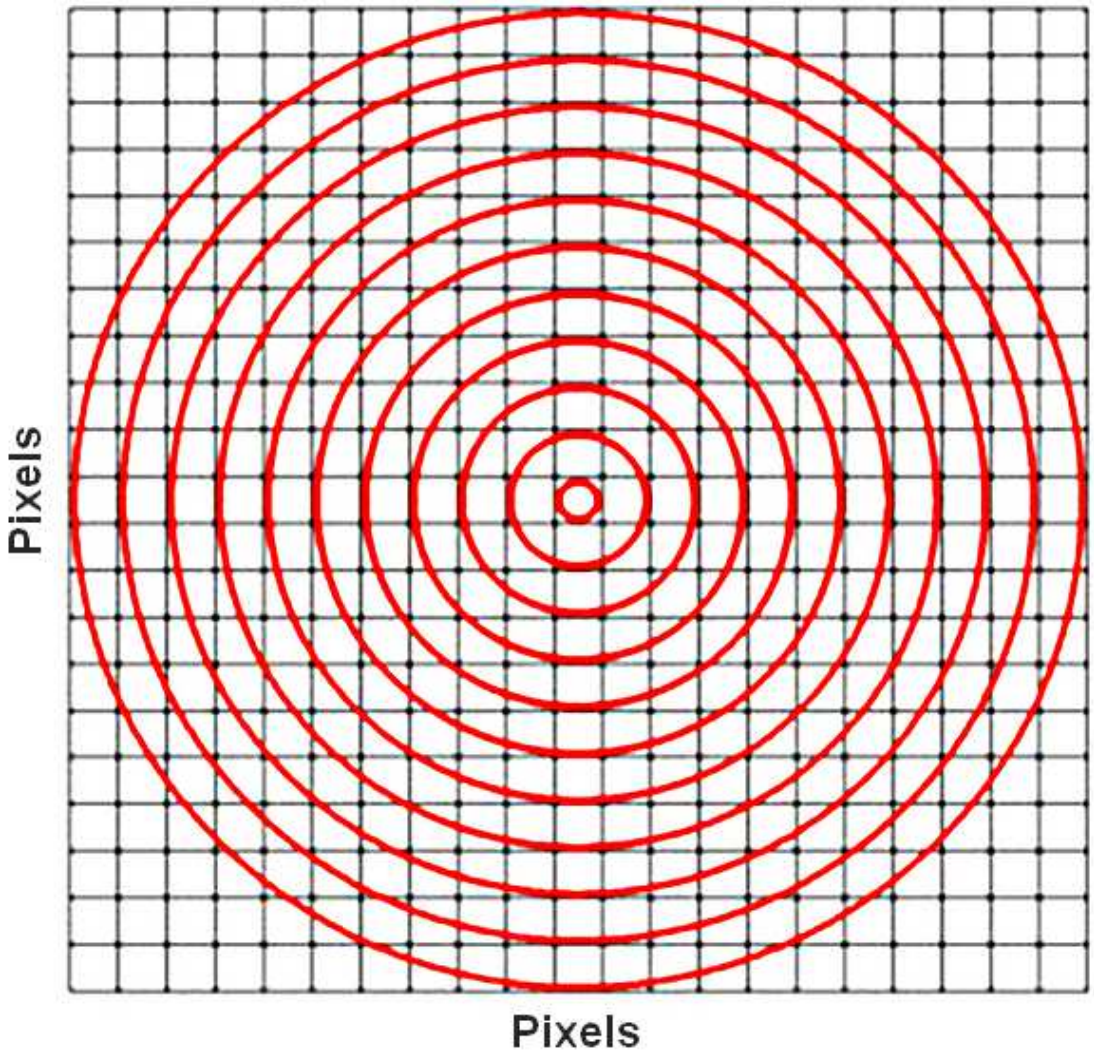


**Figure S3** The concentric ring approach description